Solid State Phenomena
ISSN: 1662-9779, Vol. 386, pp 55-62
doi:10.4028/p-MNcxv1

Submitted: 2025-05-23
Revised: 2025-12-04
Accepted: 2025-12-19
Online: 2026-03-13

Influence of Thermal Treatments on the Corrosion Behaviour of Nickel-Aluminum Bronze in Freshwater-like Aqueous Environment

Paul Linhardt[1,a], Maria Victoria Biezma[2,b], Susanne Strobl[1,c] and Roland Haubner[1,d*]

[1]Technische Universität Wien, Institute of Chemical Technologies and Analytics, Getreidemarkt 9/164-03, A-1060 Vienna, Austria

[2]University of Cantabria, Dique de Gamazo 1, 39004 Santander, Spain

[a]paul.linhardt@tuwien.ac.at, [b]biezmav@unican.es, [c]susanne.strobl@tuwien.ac.at, [d*]roland.haubner@tuwien.ac.at

Keywords: Nickel-Aluminum-Bronze, Heat Treatment, Corrosion, Freshwater.

Abstract. Nickel-Aluminium Bronze is a copper alloy with excellent corrosion resistance in marine environments. However, there are also applications of NAB in freshwater and corrosion phenomena have been observed in such cases. To explore the effect of microstructure on the corrosion behaviour, heat treatments were applied to NAB samples, which were corrosion tested in electrolytes with a composition typical for freshwater. Depending on the presence of bicarbonate, sulfate, and chloride, different kinds of corrosion attack were observed. The mayor effect lies in minimization of the β-phase amount and increasing the portion of α- and κ-phases. Corrosion promoted by sulfate is the major hazard in fresh water, while the passivating effect of bicarbonate supports localization of the attack. Chloride plays an ambivalent role; it promotes the corrosion attack but limits the progressively penetrating evolution of localized corrosion. Since the composition of freshwater has a stronger impact on the corrosion phenomena of the NAB alloy, the influence of the heat treatments is not clearly evident. Compared to seawater, heat treatments have a lesser effect on the corrosion behaviour in freshwater.

Introduction

Nickel-Aluminium Bronze (NAB) Bronzes exhibit excellent corrosion resistance and are frequently used in applications where corrosion, erosion, and cavitation can occur. This applies to both seawater and freshwater. Typical examples include ship propellers, pumps, and turbines in hydroelectric power plants [1, 2]. Due to the complex alloy composition, these bronzes have a multi-phase microstructure, which also affects the corrosion behaviour [3–6]. In this respect, some studies have been carried out previously with Manganese-Aluminium bronzes (MAB) [7–9].

The microstructures of the NAB bronzes consist primarily of three easily distinguishable phases (α, β, and κ). The α and β phases form the matrix in which the κ phase is embedded. Heat treatments make it possible to influence the phase proportions, as well as their size, geometry and distribution [10, 11]. The phase diagram (Fig. 1) [12, 13] shows, that during solidification of the bronze melt only β-phase is formed in the first step. During further cooling the β-phase decomposes into α-phase and κ-phases below 940 °C. Between 940 °C and 800 °C a ternary phase region with α-, β- and κ-phases exists. Below 800 °C the β-phase gets completely converted and α- and κ-phases are present only in the NAB microstructure. Especially the κ-phases can show different morphologies and variable compositions between Fe_3Al and NiAl [14, 15]. By quenching from 1000 °C to room temperature, the formation of a martensitic phase, referred to as β′, is described. During a subsequent heat treatment, the β′-phase decomposes into fine-grained α- and κ-phases [16].

The corrosion behaviour of NAB in seawater has been repeatedly studied [17–19], mostly related to as-cast material. Its excellent resistance to high chloride environment is based on formation of a passivating layer consisting dominantly of copper and aluminum oxides. The multiphase structure bears the risk of dealloying or selective corrosion of the most reactive (anodic) phases [20].

Conversely, corrosion of NAB in fresh water is not much discussed in literature. Nevertheless, a specific case of NAB corrosion in river water has drawn our attention to this topic [21] and the corrosion behaviour of as-cast NAB in various fresh water compositions was investigated [22]. Based on these considerations, the influence of heat treatments on the NAB´s microstructures and its influence on the corrosion behaviour in freshwater are the objectives of this study.

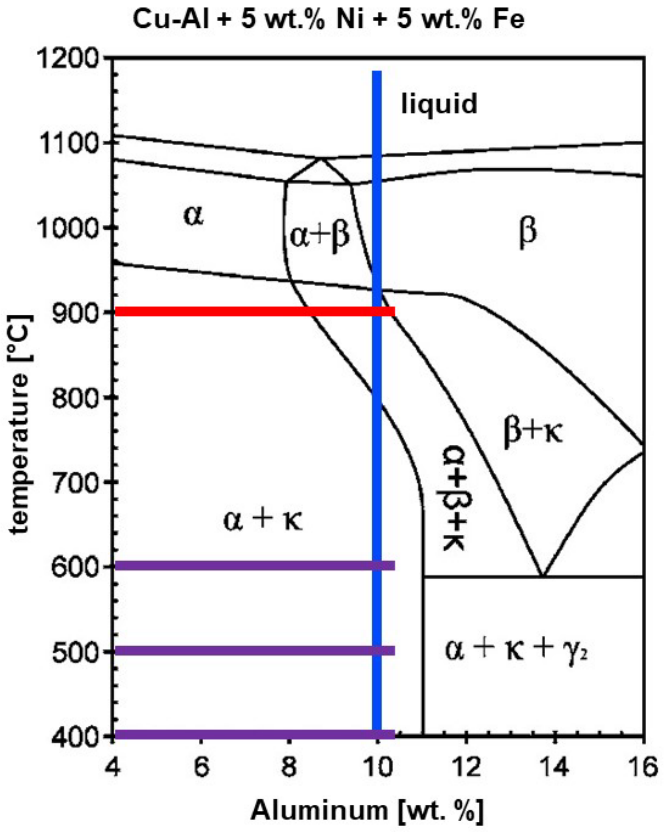

Fig. 1 Cu-Al + 5 wt.% Ni + 5 wt.% Fe phase diagram.

Experimental Procedure

NAB composition. type CuAl10Fe5Ni5 (analysis mass %: 80.53 Cu, 8.96 Al, 4.46 Fe, 4.60 Ni, 1.16 Mn, 0.07 Zn, 0.05 Sn, 0.01 Pb, 0.16 Si) (Table 1).

Heat treatments. The heat treatments were carried out in a muffle furnace, with the samples protected from oxidation by carbon grit. After annealing, the samples were quenched in water. NAB samples were solution annealed at 900 °C for 1 hour and then heat treated at 400, 500, or 600 °C for 45 min and 24 h respectively.

Metallography. The samples were embedded in epoxy resin. Metallographic preparation started with plane-grinding, followed by polishing with 9–1 μm diamond suspension. Etchant was $(NH_4)_2CuCl_4$.

Corrosion tests. Based on [22] potentiostatic corrosion testing at +194 $mV_{Ag/AgCl}$ was applied for 48 hours in solutions based on combinations of 0.5 mM SO_4^{2-}, 1 mM HCO_3^-, 0.5 mM Cl^- (Table 2). After the corrosion tests, the surfaces of the samples were examined in the SEM as well as metallographic cross sections were prepared and investigated in LOM.

Table 1 Composition of the NAB alloy CuAl10Fe5Ni5.

Element	Cu	Al	Fe	Ni	Mn	Zn	Sn	Pb	Si
wt. %	80.53	8.96	4.46	4.60	1.16	0.07	0.05	0.01	0.16

Table 2 Composition of the three electrolytes.

Electrolyte 1	Electrolyte 2	Electrolyte 3
48 mg/L SO_4^{2-}	48 mg/L SO_4^{2-} 61 mg/L HCO_3^-	48 mg/L SO_4^{2-} 61 mg/L HCO_3^- 17.5 mg/L Cl^-

Results and Discussion

Microstructural changes of NAB during heat treatments. As can be seen from the phase diagram (Fig. 1) at 900 °C, the 3 phases α-, β- and κ- are present.
Figure 2 shows the microstructure of the sample annealed and quenched at 900 °C. The light areas correspond to the α-phase, and the dark brown areas correspond to the β-phase. The κ-phases appear bright gray, with larger aggregates in the α-phase and smaller precipitates in the β-phase.
Starting with the sample annealed at 900 °C, annealing at lower temperatures should result in a transformation of the β-phase into the α-phase and κ-phases. This transformation is more slowly at lower temperatures (Fig. 3), while higher temperatures result in coarsening of the phases.

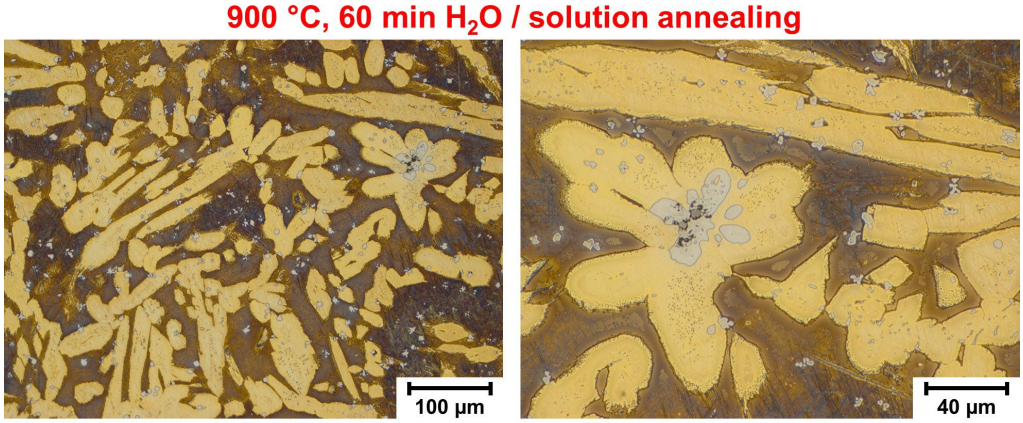

Fig. 2 Microstructures of the at 900 °C heat-treated NAB samples. Etchant $(NH_4)_2CuCl_4$.

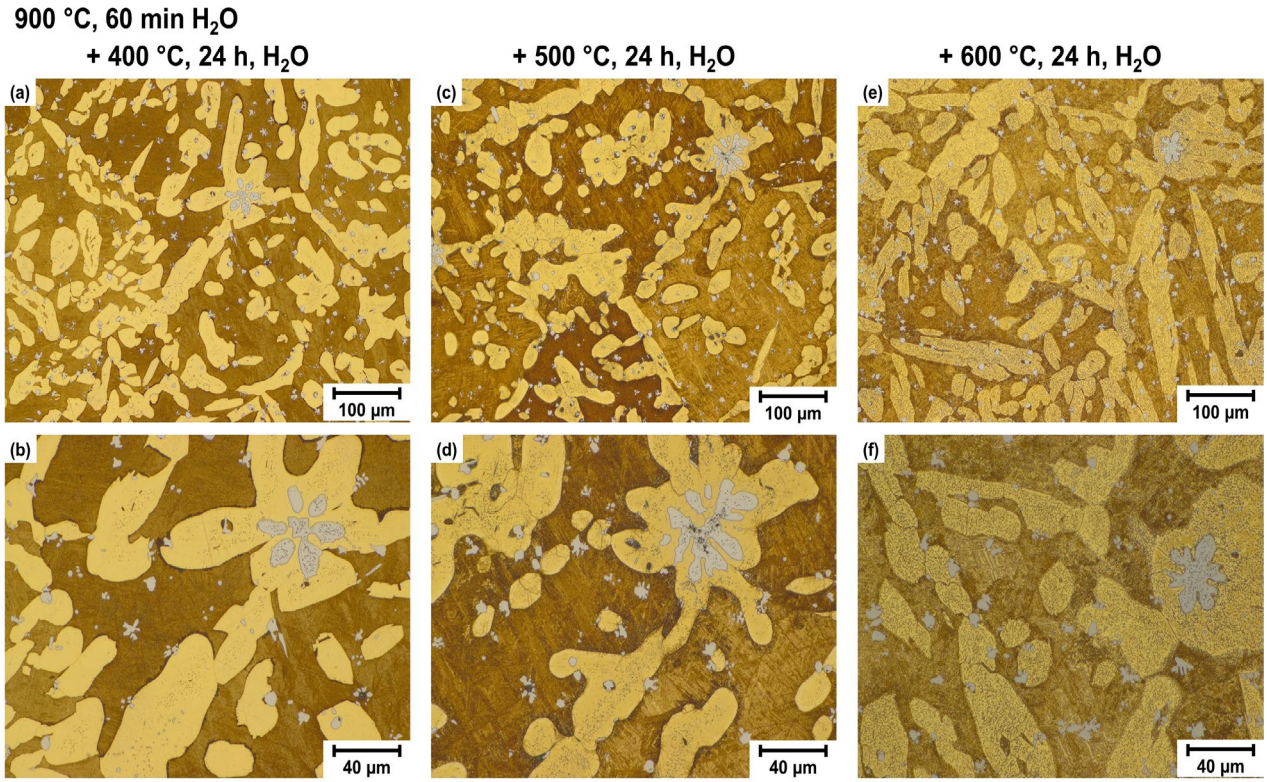

Fig. 3 Microstructures of the heat-treated NAB samples. Etchant $(NH_4)_2CuCl_4$.

In the sample annealed at 400 °C the α-phase and κ-phases appear unchanged, but darker and lighter areas are visible in the β-phase regions (Fig. 3a, b), and precipitation of fine κ-phase is observed. In a sample annealed at 500 °C, the darker and lighter regions of the original β-phase are contrasting better (Fig. 3c, d). After annealing at 600 °C, very fine κ-precipitates are visible additionally, in both the original β-phase and α-phase regions (Fig. 3e, f).

Potentiostatic electrochemical measurements. In sulfate electrolyte (electrolyte 1), a significant reduction in the corrosion current was observed as a result of the heat treatments compared to the solution-annealed sample (Fig. 4a). The attack appears as areas of rather uniform corrosion with adhering corrosion products with the solution-annealed sample (Fig. 5a). This is reflected in the rather steady current trend reached finally. In contrast, pitting-like corrosion was observed with all samples, corresponding with increasing trends of the currents, all at similar level. The attack is likely to have occurred preferentially in the vicinity of the large κ-aggregates within the α-phase (Fig. 5b–d).

In the sulfate-carbonate electrolyte (electrolyte 2), the corrosion currents were similarly low in all samples (Fig. 4b). This can be attributed to the effect of the carbonate, which forms a protective layer. Pitting-like corrosion, again corresponding with increasing current trends, was observed. The halos around the pits consist predominantly of Al corrosion products. Pitting corrosion is likely to originate from areas with κ-phase (Fig. 5e–h).

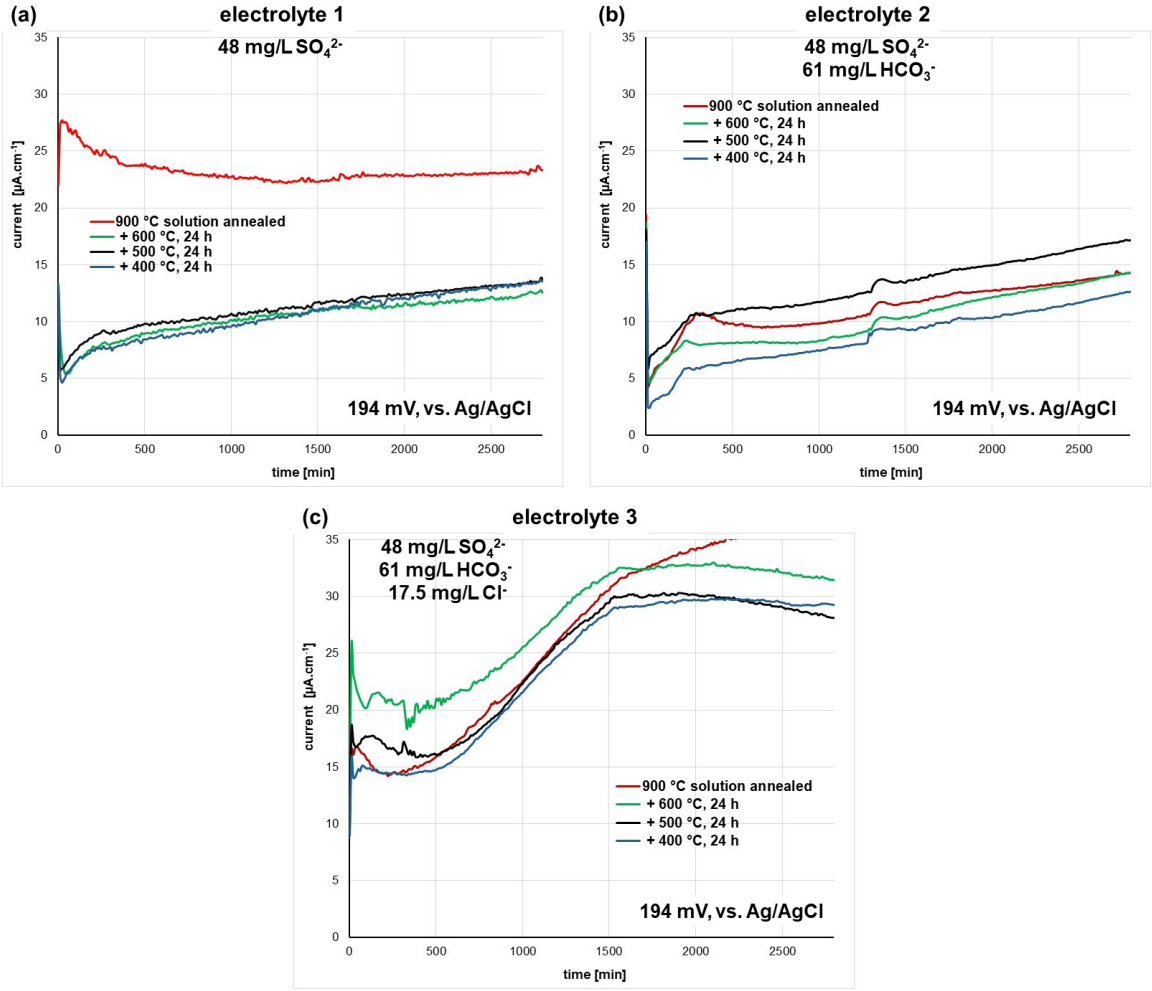

Fig. 4 Trends of current densities during on potentiostatic corrosion testing of heat treated NAB samples in three electrolytes.

If chloride was also present in the electrolyte in addition to sulfate and carbonate (electrolyte 3), the effects of the heat treatments were minimal, but the corrosion currents were significantly increased (Fig. 4c). These samples had poorly protective layers of corrosion products on the surfaces, which mainly contained aluminum compounds. Aluminum from the alloy is the most reactive element and corrodes easier. The attack appears as a kind of localized etching; no penetrating pitting was observed (Fig. 5i–l). This is reflected in increasing current trends in the beginning, which flatten and even get decreasing later on.

Cross sections of the corroded samples. Cross sections were taken from some samples after the potentiostatic corrosion tests to determine the degree of corrosion attack. Samples from the tests with electrolyte 3 were used for this purpose, as the corrosion current was highest in these tests and therefore the most metal loss from corrosion is expected (Fig. 6).

In general, it can be said that the localized corrosion attack was minor. It should also be noted that with localized corrosion, corrosion spots may not be easily detected in the metallographic section. In the sample annealed at 500 °C, corroded spots are visible that extend approximately 20 µm below the surface (Fig. 6a). The results for the sample annealed at 400 °C are similar, but dealloying, presumably due to corrosion of the β-phase, is also evident here (Fig. 6b). Furthermore, there are spots where the attack extends up to 50 µm below the surface, as well as crack-like phenomena (Fig. 6c).

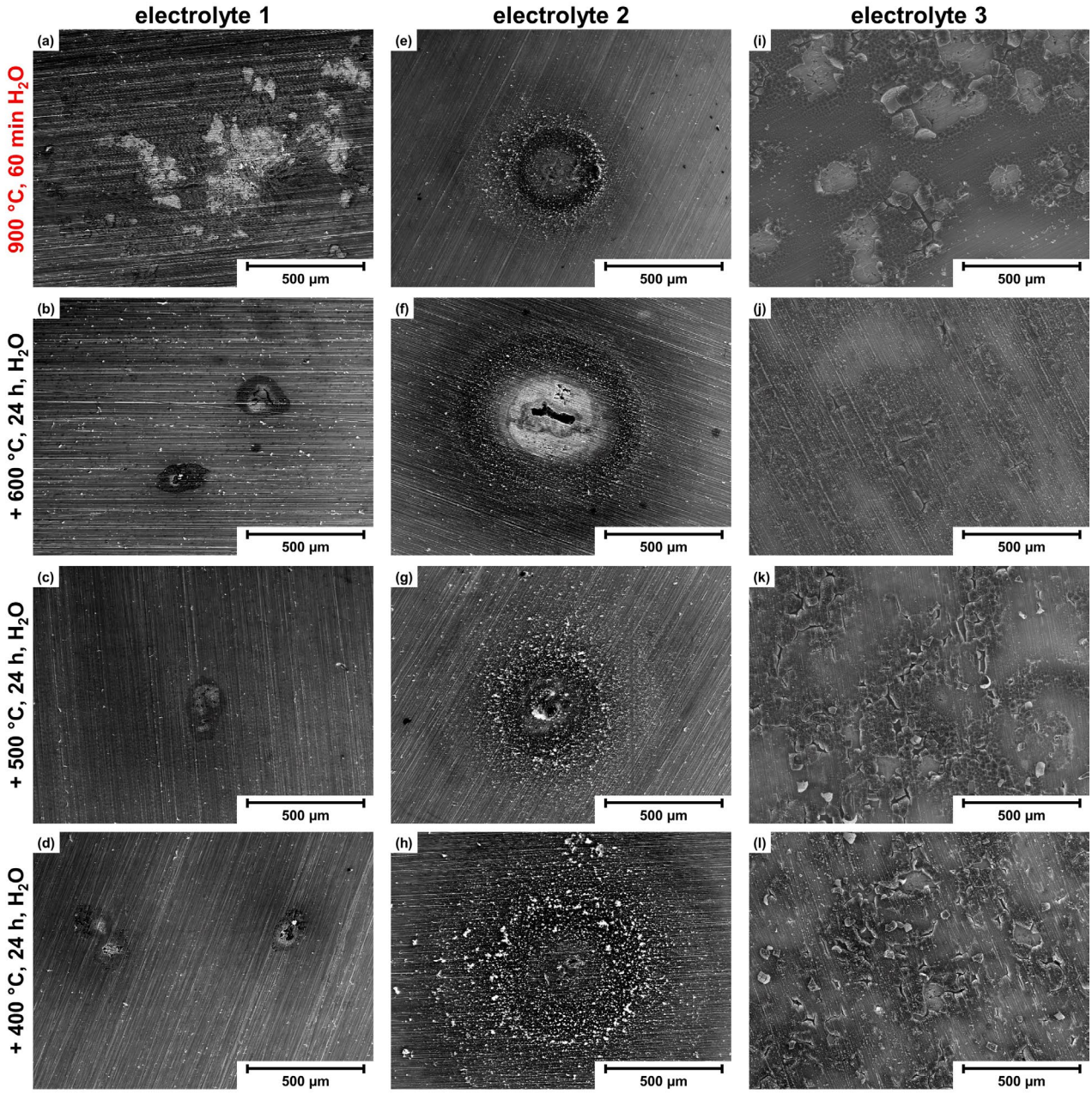

Fig. 5 Surfaces of the NAB samples after the potentiostatic corrosion tests in different electrolytes (SEM-BSE).

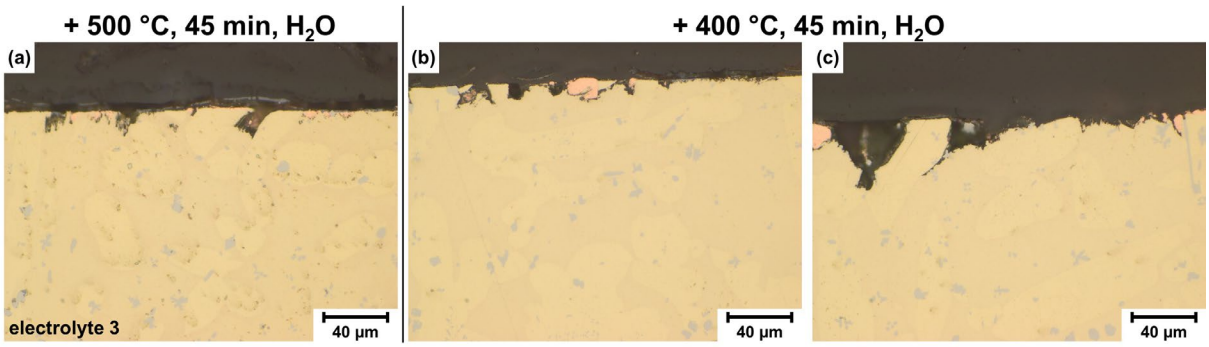

Fig. 6 Metallographic cross-sections of NAB samples after potentiostatic corrosion tests.

Summary

Nickel-Aluminium Bronze samples were tested for their corrosion resistance in synthetic freshwater after different heat treatments. Depending on the composition of this medium, different kinds corrosion attack was observed.

The influence of heat treatments on corrosion in freshwater is small compared to seawater [10]. In freshwater, the water composition primarily determines the corrosion behaviour.

The main effect of the heat treatments lies in minimization of the β-phase amount and increasing the amount of κ-phases and α-phase.

Corrosion promoted by sulfate is the major hazard in fresh water, while the passivating effect of bicarbonate supports localization of the attack. Chloride plays an ambivalent role; it promotes the corrosion attack, but limits the progressively penetrating evolution of localized corrosion. These observations agree with the findings reported previously [22].

Acknowledgements

The authors would like to thank the TU Wien Library for the financial support through its Open Access Funding Program.

References

[1] Z. Qin, Q. Zhang, Q. Luo, Z. Wu, B. Shen, L. Liu, W. Hu, Corros. Sci., 139 (2018) 255-266.

[2] P. Linhardt, S. Strobl, J. Böhm, M.V. Biezma Moraleda, R. Haubner, Pract. Metallogr., 58 (2021) 72-82.

[3] P. Brezina, Int. Met. Rev., 27 (1982) 77-120.

[4] E.A. Culpan, G. Rose, J. Mater. Sci., 13 (1978) 8, S. 1647-1657.

[5] P. Linhardt, S. Strobl, J. Böhm, M.V. Biezma Moraleda, R. Haubner, Pract. Metallogr., 58 (2021) 72-82.

[6] F. Hasan, A. Jahanafrooz, G.W. Lorimer, N. Ridley, Metall. Trans. A, 13A (1982) 1337-1345.

[7] M.V. Biezma, O. Gómez de la Rasilla, R. Haubner, P. Linhardt, Pract. Metallogr., 59, 5 (2022) 236-250.

[8] P. Linhardt, M.V. Biezma, S. Strobl, R. Haubner, Solid State Phenomena, 341 (2023) 25-30.

[9] R. Haubner, S. Strobl, G. Ball, P. Linhardt, M.V. Biezma, Pract. Metallogr., 61 (2024) 769-782.

[10] J. Böhm, P. Linhardt, S. Strobl, R. Haubner, M.V. Biezma Moraleda, Materials Performance and Characterization, 5 (2016) 689-700.

[11] I. Cobo Ocejo, M.V. Biezma Moraleda, P. Linhardt, Metals, 12 (2022) 380.

[12] Kupfer-Aluminium-Legierungen, Informationsdruck i.6, Deutsches Kupferinstitut, Auflage 03/2010.

[13] B.P. Pisarek, Archives of foundry engineering, 13 (2013) 72-79.

[14] E.A. Culpan, G. Rose, Journal of Material Science, 13 (1978) 1647-1657.

[15] R. Thomson, J.O. Edwards, The Kappa-Phase in Nickel-Aluminium Bronze, Part 2: Cast Microstructures and Properties, in AFS Transactions (1978) 395-400.

[16] P. Brezina, International Metals Reviews, 27 (1982) 77-120.

[17] J.A. Wharton, R.C. Barik, G. Kear, R. J. K. Wood, K.R. Stokes, F.C. Walsh, Corrosion Science, 47 (2005) 3336-3367.

[18] A. Al-Hashem, W. Riad, Materials Characterization, 48 (2002) 37-41.

[19] E.A. Culpan, G. Rose, British Corrosion Journal, 14 (1979) 160-166.

[20] J.A. Wharton, K. R. Stokes, Electrochim. Acta, 53 (2008) 2463-2473.

[21] P. Linhardt, Materials and Corrosion, 66 (2015) 1536-1541.

[22] P. Linhardt, S. Kührer, G. Ball, M.V. Biezma, Materials and Corrosion, 69 (2018) 358-364.

The publication of this article was funded by the TU Wien 10.13039/501100004729